Angle-resolved velocity distributions of excited Rh atoms ejected from ion-bombarded Rh{100}

Dan N. Bernardo, Mohamed El-Maazawi, Roya Maboudian, Zbigniew Postawa,[a)]
Nicholas Winograd, and Barbara J. Garrison
Department of Chemistry, The Pennsylvania State University, University Park, Pennsylvania 16802

(Received 30 March 1992; accepted 7 May 1992)

The distributions of metastable excited state ($^4F_{7/2}$) and ground state ($^4F_{9/2}$) Rh atoms ejected from Ar^+-bombarded Rh{100} are experimentally determined as a function of ejection velocity and angle. Corresponding theoretical predictions are made by incorporating a nonradiative deexcitation model into molecular dynamics simulations of the bombardment process. There is good agreement between the experimental and theoretical distributions. The simulations show that a fraction of the ejected atoms are excited via collisions 1–20 Å above the surface, and that these atoms make a significant contribution to the excited atom yield at low ejection velocities.

I. INTRODUCTION

The impact of an energetic ion on a solid surface initiates a complex and often mysterious sequence of momentum transfer, atomic motions, and electronic excitations within the solid. During such an event atoms and clusters are ejected from the target. These particles may be in ground, electronically excited, or ionized states and are ejected with various velocity and angular distributions. The analysis of these distributions can provide clues to understanding the processes by which these various species are produced. For some systems[1,2] the ejection of atoms in their ground state is reasonably understood, particularly since a classical description of the atomic motions is sufficient to explain the observed experimental distributions.

The study of the processes whereby excited atoms are ejected presents the additional challenge of accounting for the electronic excitations in addition to describing the atomic motions. This excitation process has been investigated for many years.[3–17] It has been suggested that these atoms are produced via a two-step mechanism involving (a) formation of excited atoms within the collision cascade, and (b) relaxation of the initial excitation.[18,19] With use of this model, the excitation probability is predicted to vary with velocity as $\exp(-A/av_\perp)$, where A and a are constants and $v_\perp$ is the component of velocity normal to the surface. Over the years, this relation has been a reasonable representation of the experimental data.

Some angle-resolved velocity distributions of Rh atoms in the ground ($^4F_{9/2}$) and first electronic excited ($^4F_{7/2}$) states ejected from Rh{100} due to keV particle bombardment have been recently measured.[17] These data are valuable for testing current electronic excitation theories and possibly stimulating the development of new ones. These recent experimental results are particularly significant for two reasons. First, the intensities of excited atoms (dN^*/dv) and ground state atoms (dN/dv) were measured for the two main azimuthal angles of ejection (see Fig. 1). This is important since the test of existing theories becomes more stringent when comparisons are made with experimental data over specific azimuthal angles of ejection. Second, the ratios of excited state to ground state distributions $(dN^*/dv)/(dN/dv)$ were found to exponentially decrease with $1/v_\perp$ for high values of $v_\perp$. At low values of $v_\perp$, $(dN^*/dv)/(dN/dv)$ leveled off at some constant value. This change in the behavior of $(dN^*/dv)/(dN/dv)$ with $v_\perp$ suggests the possible existence of different excitation mechanisms in the two velocity regimes.

In this paper we present extensive velocity-resolved angular distributions of Rh atoms ejected from Rh{100} in the ground state, $^4F_{9/2}$, and the next higher-lying excited state, $^4F_{7/2}$, which has an excitation energy of 0.2 eV. We show that a combination of the nonradiative deexcitation approach with realistic atomic trajectories predicts distributions which are in good agreement with experimental results. The use of molecular dynamics simulations reveals some collisional mechanisms which have not been apparent in simpler implementations of the nonradiative deexcitation model. For example, atomic collisions 1–20 Å above the surface are found to be important for excitations at low velocities. On the other hand, atoms ejecting at high velocities and at certain angles are deflected or reexcited by neighboring atoms. It is mechanisms such as these which account for the experimentally observed variations of the distributions with ejection velocity and angle.

II. THEORY

In this section we develop an approach for calculating the velocity- and angle-dependent distributions of Rh atoms ejected in their ground and excited states due to ion bombardment. In simulating the ejection of these species, one must treat both the atomic motions and the electronic excitations. The choice of a model for electronic excitation depends in part on the approach used to calculate the atomic motions. It has been shown[1,2] that the atomic motions and velocity and angular distributions are well described by molecular dynamics simulations. This approach considers the target to be a small crystallite consisting of

[a)]Permanent address: Institute of Physics, Jagellonian University, Krakow ulica Reymonta 4, Poland.

 0021-9606/92/173846-09$006.00

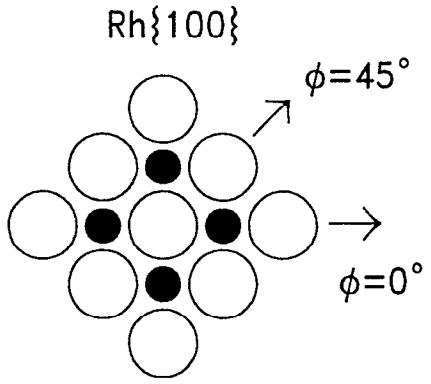

FIG. 1. Top view of the Rh{100} face. The main azimuthal angles are shown. Solid circles represent the first layer atoms and dotted circles indicate second layer atoms.

several hundred atoms and calculates the interatomic forces and atomic motions over a period of time. The accompanying model for electronic excitations must be able to calculate excitations in this system (i.e., 700–1000 atoms with no symmetry constraints), and its algorithm must be sufficiently fast to allow the simulation of a few thousand ion bombardment trajectories in a reasonable amount of time. It is these constraints which rule out the use of more elaborate and computationally intensive models for the calculation of excitation probabilities. We have thus elected to use an empirical approach which, like more advanced models, allows the examination of the relation between atomic collisions and electronic excitations.

There exist phenomenological approaches for the calculation of distributions of atoms in the excited state. However, theoretical approaches on the atomic scale usually do not calculate the excited-state distributions directly. The parameter of choice is instead the excitation probability P, which is the ratio of the number of excited atoms to the total number of atoms. The behavior of P has been described by the nonradiative deexcitation approach[4–8]

$$P(v)=P_0(v)R(v), \tag{1}$$

where $P_0(v)$ is the initial value of the probability of a sputtered atom with velocity v being in the excited state and $R(v)$ is the probability that the excited atom survives nonradiative decay.

The extent of nonradiative deexcitation can be evaluated using a model which has been used to describe inner-shell excitations in ion-bombarded Al.[20,21] The excitation process is considered to occur when the distance between two atoms (either two target atoms, or a target atom and a bombarding ion) becomes less than a threshold distance $r_{\rm th}$. At this point the excitation probabilities for these atoms are set to the initial value P_0. This excitation probability does not depend on whether the atom is excited before the collision. When the excitation process is over, the excitation probability is subjected to the time-dependent decay

$$dP/dt=-P/\tau, \tag{2}$$

where τ is the lifetime. The lifetime depends on the extent of interaction with the substrate electrons. This interaction is considered to be constant up to some height z_s, after which it exponentially decreases with some factor γ. In other words, τ may be defined as

$$\tau=\tau_s \quad \text{for} \quad z\leqslant z_s, \tag{3}$$

and

$$1/\tau=(1/\tau_s)\exp[-\gamma(z-z_s)] \quad \text{for} \quad z>z_s, \tag{4}$$

where z is the distance between the atom and the original plane of first layer atoms. Note that the lifetime in the gas phase (i.e., at large z) approaches infinity. We consider this to be a reasonable limit since the $^4F_{7/2}$ excited state, being a fine-structure component of the ground state multiplet, is metastable.

Our approach to calculating the excitation probability uses several parameters. The determination of their values is discussed in Sec. IV B. Some of these values are based on *ab initio* electronic structure calculations while others are based on experimental data.

It is interesting to note that the parametrization of the lifetime does not involve any assumptions regarding the velocity or angles of ejection. The assumption of a constant value of $v_\perp$ over the ejection trajectory has been used in previous studies in order to obtain a simple relation for $R(v)$. If an atom is excited at $z=0$ Å and subsequently ejects with a constant $v_\perp$, then the survival probability is [see Eq. (1)]

$$R(v)=\exp(-A/av\cos\theta)=\exp(-A/av_\perp), \tag{5}$$

where v is the total velocity, θ is the polar angle of ejection, and A/a is the decay coefficient. This relation has been observed in numerous experiments, although deviations from this relation have been found at low ejection velocities.[10,22–27] These deviations have been attributed to the surface binding energy, which causes $v_\perp$ to take on higher values in the near-surface region before the atom actually ejects.

As mentioned earlier, molecular dynamics computer simulations are used to examine the effect of realistic trajectories on the excitation process. The simulation of the atomic motions during a sputtering event has been described in detail elsewhere.[1] Instead of repeating its description here, we will only emphasize aspects of the method which are most important in deducing the angular and velocity dependencies of the excitation probability. First, a many-body potential that provides a realistic description of the surface binding energy is used. In this case an ejecting atom does not experience a purely height-dependent, planar potential, but one which is sensitive to the number and distances of its neighboring atoms.[2] Second, the treatment of individual atomic motions allows the examination of lattice disruption and development of increasing anisotropy of the system over the course of a collision cascade. Third, it has been shown[2] that simulations of the ion bombardment of Rh{100} yield angular distributions of ejected atoms which are in good agreement with experimental findings.

The molecular dynamics simulations yield $N_t(v,\theta,\phi)$, the total number of atoms ejected with velocity v and polar and azimuthal angles of θ and ϕ, respectively. The electronic excitation model gives the excitation probabilities for these atoms. The number of atoms in the excited state is obtained by

$$N^*(v,\theta,\phi)=N_t(v,\theta,\phi)P_{\text{ave}}(v,\theta,\phi), \tag{6}$$

where $P_{\text{ave}}(v,\theta,\phi)$ is the average of the excitation probabilities of the individual atoms.[28] Since this theoretical approach considers the system to consist solely of atoms in the ground and first electronically excited states, the number of atoms in the ground state is given by

$$N(v,\theta,\phi)=N_t(v,\theta,\phi)[1-P_{\text{ave}}(v,\theta,\phi)]. \tag{7}$$

The ratio of excited state to ground state distributions is then

$$(dN^*/dv)/(dN/dv)\approx N^*(v,\theta,\phi)/N(v,\theta,\phi). \tag{8}$$

The shortened notation on the left-hand side of the equation will be used in the rest of the paper.

III. EXPERIMENT

In this section various aspects of the experiment that are of importance to the present work are briefly mentioned. The Rh sample is an optically polished single crystal of 99.99% purity oriented to within 0.5° of the (100) face. The cleaning procedure[2] and experimental setup[29] have been described elsewhere. The measurement procedure will be briefly described here.

Measurements are performed in an ultrahigh-vacuum chamber (2×10^{-10} Torr base pressure) equipped with a low-energy electron diffraction and Auger surface analysis system. A 200 ns pulse of 5 keV Ar^+ is focused, at normal incidence, onto a 2 mm spot on the sample. A given time after the ion impact, a ribbon-shaped laser pulse is used to ionize the atoms found in a small region above the surface. The time delay between the ion impact and the laser pulse defines the time of flight of the probed species. The multiphoton resonance ionization scheme for both ground- and excited-state atoms consists of a one-photon excitation to the intermediate level ($^2F^0_{7/2}$) followed by a second photon absorption which induces ionization.[16] The ionized particles are then accelerated toward a microchannel plate detector–phosphor screen assembly which displays the relative positions of the ejected particles. For a typical measurement, 30–60 images, each corresponding to a different time of flight, are collected and analyzed to yield an intensity map of kinetic energies and takeoff angles.

IV. RESULTS AND DISCUSSION

The experimental results, the calculation of the parameters used in the model, and the results of the simulations are discussed in that order. Two simulation systems are considered. These are (a) the ideal case of a single atom being ejected from an undisturbed perfect crystal surface, and (b) the production of ejected atoms via ion bombardment of the target and disruption of the crystal structure. The ideal case allows one to isolate portions of the atom–surface interactions which influence the excitation process. The second case is important for several reasons. First, it provides a statistical picture of the angular and velocity dependence of P. Second, it shows how the excitation process is affected by the collision cascade and disruption of the target structure. Third, it illustrates the importance of collisions between ejected atoms.

A. Experimental results

The ratio of the distribution of excited state atoms to the distribution of ground state atoms, $(dN^*/dv)/(dN/dv)$, is shown as a function of $1/v_\perp$ in Figs. 2(a) and 2(b). Data for two azimuthal directions (ϕ) and six polar angle (θ) intervals are displayed. Results for Rh atoms ejected along $\phi=0°$ (the open ⟨100⟩ crystallographic direction) are shown in Fig. 2(a), while results for atoms ejected along $\phi=45°$ (the close-packed ⟨110⟩ direction) are shown in Fig. 2(b). There are features of the distributions which are common to all the plots. First, at high velocities the excitation probability varies exponentially with $1/v_\perp$, with slope A/a. However, there is some variation of the slope with the polar and azimuthal angles of ejection. Along the $\phi=45°$ azimuth, A/a is observed to slightly increase with polar angle for $\theta<40°$. For the $\phi=0°$ azimuth, this ratio is independent of the polar angle. Second, at low velocities the ratio $(dN^*/dv)/(dN/dv)$ levels off at some constant value D_l. However, the value of D_l is dependent on the polar and azimuthal angles of ejection. For $\phi=0°$, D_l appears to decrease with increasing polar angle of ejection. For $\phi=45°$, D_l remains constant for all values of θ. It must be pointed out that the transition in the behavior of $\log[(dN^*/dv)/(dN/dv)]$ from being linear in $1/v_\perp$ to being constant is not gradual but occurs abruptly at values of $v_\perp=(4\times10^5)$–(5×10^5) cm/s, the exact value depending on the angles of ejection.

B. Determination of parameters in the model

As outlined in Sec. II, the model has five parameters whose values must be determined before performing any calculations. When possible, attempts are made to place an experimental or theoretical basis behind the choice of their values.

The value of P_0, the initial excitation probability, is based on the experimental data. In the limit of infinite velocity, an ejected atom should retain its initial excitation probability. Extrapolation of the $\theta<10°$ data (which is the same for both azimuthal directions) in Fig. 2 to $1/v_\perp=0$ yields a value of $P_0=0.76$. It must be pointed out that only trajectories normal to the surface are used in this parametrization. It will be shown later that particles ejected with $\theta>30°$ undergo additional excitations which would obscure the effects of the initial excitation.

The lifetime of the excited state τ is affected by the three parameters z_s, τ_s, and γ [cf. Eqs. (3) and (4)]. From electronic structure calculations[30,31] the electron density of the Rh 5s orbital is determined to have a maximum at 1.2 Å. This is used to assign $z_s=1.2$ Å. The electronic structure calculations also show that the electron density for the

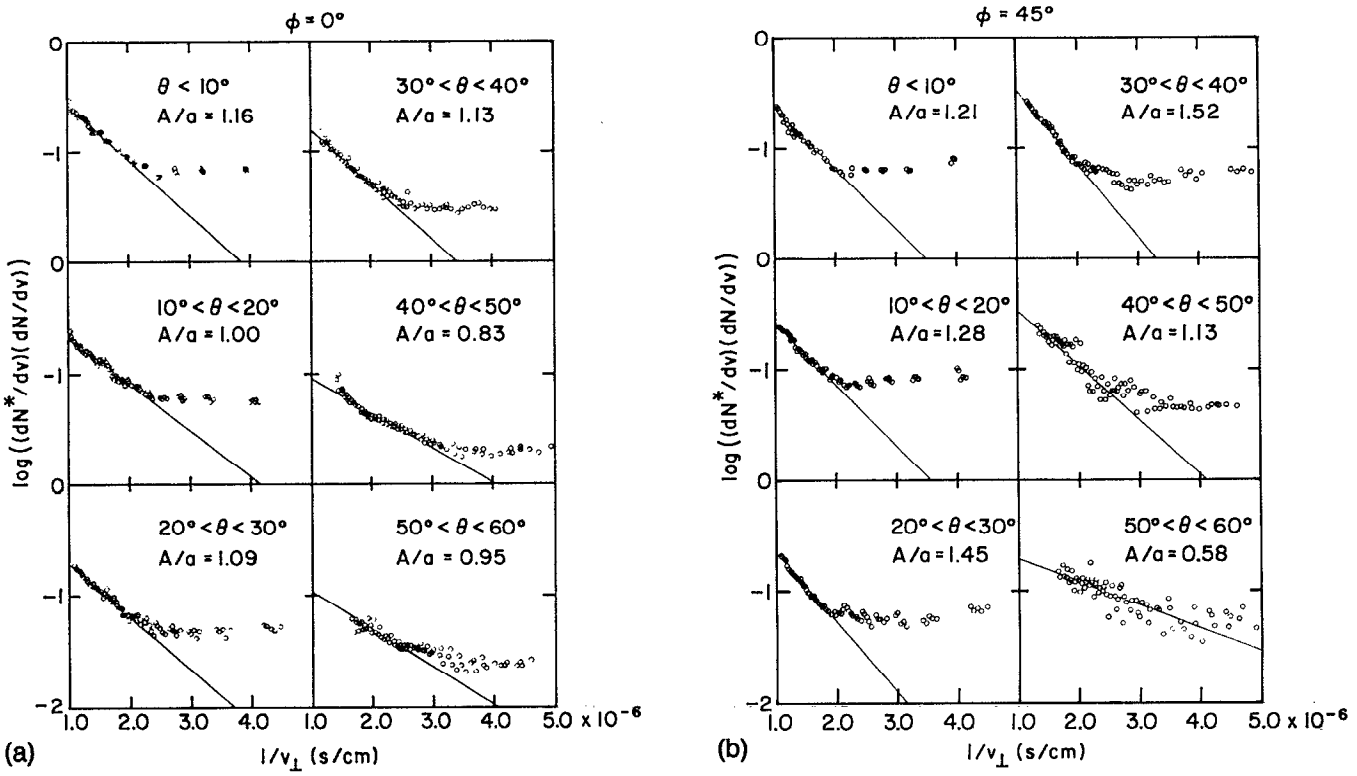

FIG. 2. Experimental results. The ratios of velocity distributions $(dN^*/dv)/(dN/dv)$ are given for two azimuthal directions and six polar angle intervals. (a) $\phi=0°$ (open, ⟨100⟩ direction); (b) $\phi=45°$ (close-packed, ⟨110⟩ direction). Values of A/a (in units of 10^6 cm/s) for each plot are also given.

valence orbitals of Rh becomes negligible ($<0.1\%$ of its maximum value) at $z=5$ Å. The assignment of $\exp[-\gamma(z-z_s)]=0.001$ at this value of z leads to $\gamma=1.82$ Å^{-1}.

The value for τ_s is obtained by imposing the requirement that the results of the ideal case calculations (for a single particle going straight up) match the experimental results (at $\theta=0°$) at the highest observed experimental velocity (1×10^6 cm/s). This requirement yields $\tau_s=8.16$ fs.

A suitable basis for choosing r_{th}, the threshold distance for excitation, could not be found. Studies on other systems[21] have attempted to base this parameter on electronic level crossing distances.[32] However, these electronic structure calculations apply to gas-phase collisions, and it is uncertain whether such results can be extended to collisions within the solid. This is especially true for the excitation of valence electrons (such as those involved in our system) since these electrons are quite sensitive to the atomic environment. We instead opt for an arbitrary assignment of the value of r_{th} that is less than the experimentally known interatomic distance in bulk Rh (Ref. 33) (2.69 Å) and the theoretically determined distance in the Rh dimer[34] (2.67 Å). A choice of this nature ensures that there would be no excitation in the bulk or in clusters[35] at their equilibrium geometries. Since the excitation is of low energy (0.2 eV), small values of r_{th} must not be used to avoid thresholds for far more energetic collisions. An assignment of $r_{th}=1.85$ Å meets these criteria and allows excitations to occur even in low-energy (a few eV) collisions. Note that this value of r_{th} is larger than the values (0.52–0.65 Å) used in simulations of inner shell excitations in Al.[20,21]

C. Theoretical results

All simulations are performed on a model Rh{100} crystallite consisting of 867 atoms distributed among six layers. Potential EAM-A (Ref. 1) is used to describe the interatomic forces between target atoms. The target is bombarded with a 3 keV argon ion at normal incidence. The Rh–Ar interaction is described using a Molière potential.[1] For simplicity the same value of r_{th} is used for Rh–Rh and Ar–Rh excitations. Edge atoms are not counted in the list of sputtered atoms since the decreased atomic density at a crystallite edge leads to questionable values of P for these atoms. As in previous studies using molecular dynamics simulations, the final positions and velocities of ejected atoms are recorded. In addition, the final values of P and heights at which the atoms are last excited, z_t, are recorded.

Simulations using the above computational details are first completed for the ideal case of the ejection of a single surface atom from an otherwise perfect crystal surface. These simulations eliminate the presence of other ejecting atoms and thus allow isolation and examination of the effects of specific atom–surface interactions on the excitation process. In calculations on this system a surface atom is

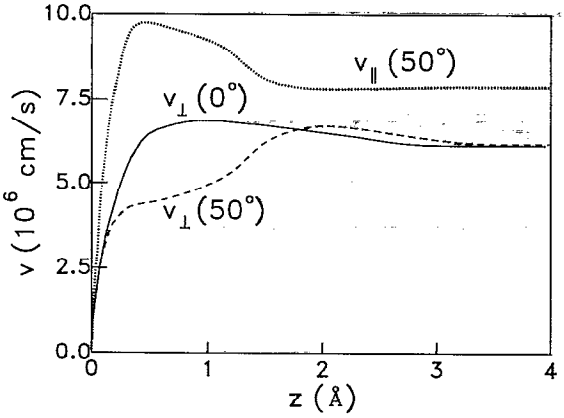

FIG. 3. Variation of velocity with height for the two ideal case trajectories with polar angles of ejection of $\theta=0°$ and $\theta\approx50°$. Ejection in the latter trajectory is along the $\phi=0°$ azimuth. The normal component of the emission velocity is shown for $\theta=0°$ and $\theta\approx50°$ as solid and dashed lines, respectively. The dotted line indicates the component of velocity parallel to the surface for the case of $\theta\approx50°$.

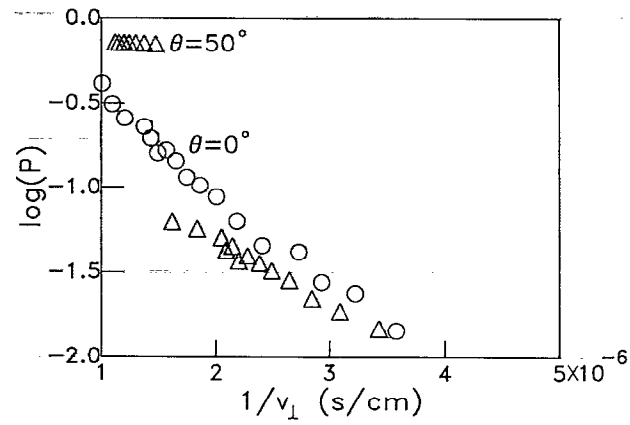

FIG. 5. Excitation probabilities obtained for the ideal case of a single atom ejecting from a perfect crystal face. Circles refer to an ejection trajectory normal to the surface ($\theta=0°$), while triangles denote an ejection trajectory with $\theta\approx50°$ along the $\phi=0°$ azimuth.

struck by another atom directly below it, and ejects with a trajectory normal to the surface. The velocity and position of the ejecting atom over the course of the trajectory were recorded.

The variation of the velocity for this particle which is ejected with $\theta=0°$ is shown in Fig. 3. Its velocity rapidly increases to some maximum value v_{max} before decreasing to its observed final value of $v_\perp$. This decrease in velocity is due to the presence of the surface binding energy which the atom must overcome before it can leave the surface. The relationship between $1/v_{max}$ or $1/v_\perp$ and P is shown in Fig. 4. The dependence of $\log(P)$ on $1/v_{max}$ is linear. The relationship between $\log(P)$ and $1/v_\perp$, on the other hand, exhibits some curvature which becomes more pronounced at low velocities. This relation has been referred to as the binding energy effect.[23,24] Comparison with the experimental data for $\theta<10°$ shows that these ideal case predictions reproduce neither the low-velocity level part of the experimental data nor the relatively sharp transition in behavior from being exponential in $1/v_\perp$ to being constant. This suggests that binding energy arguments alone cannot account for the observed behavior.

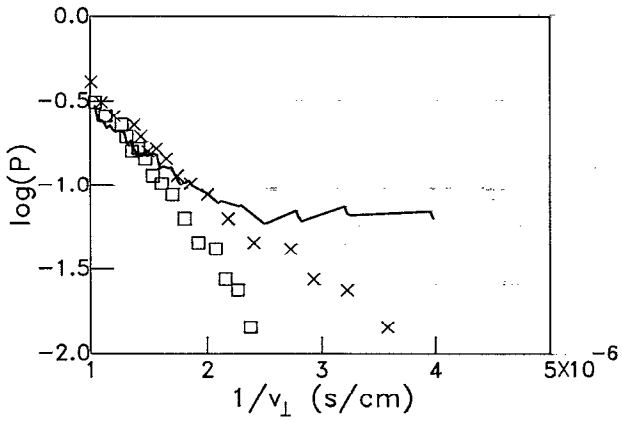

FIG. 4. Excitation probabilities obtained for the ideal case of an atom ejecting from a perfect crystal face with trajectory normal to the surface ($\theta=0°$). Squares denote the relationship between $\log(P)$ and $1/v_{max}$. Crosses indicate the variation of $\log(P)$ with $1/v_\perp$. Experimental results for $\theta<10°$ are indicated by the solid line.

The simulation using this ideal case also reveals some additional aspects of the initial excitation process. Theoretical treatments usually assume that the atom is excited at the surface (i.e., at $z=0$ Å). Our calculations indicate that this is not the case even for this idealized model. The surface atom is set into motion by a collision with the atom directly below it. The two atoms initially come into contact (we define "contact" as an event where the interatomic distance is less than r_{th}) when the surface atom is at $z\approx0$ Å. They remain in contact for some time during which the velocity of the surface atom increases. When contact is broken (at which point the initial excitation starts to decay), the atom is at some distance z_t above the surface. For example, $z_t=0.32$ Å for a collision which results in a final velocity of 5×10^5 cm/s. The production of a faster ($v_\perp=1\times10^6$ cm/s) ejected particle requires a more energetic collision in which the initial excitation ends at a height of $z_t=0.77$ Å. This suggests that the integration of Eq. (2) to yield the final value of P should not always be performed over times corresponding to the height interval $(0,\infty)$. Furthermore, if the deexcitation process starts some distance above the surface, the final value of P becomes greater than that of the case where $z_t=0$ Å since, in this case, the excited atom spends less time interacting with the solid.

After studying the ejection of an atom with a trajectory normal to the surface, we now examine the effects of nonzero polar angles of ejection on the excitation probability. We have calculated P for the case of a single atom ejecting with $\theta\approx50°$ along the $\phi=0°$ azimuth, but with the same range of $v_\perp$ as in the previous case. If it is assumed that $v_\perp$ remains constant over the ejection trajectory, then the $\log(P)-1/v_\perp$ plot should be identical to that of the previous case (with $\theta=0°$). Comparison of results in Fig. 5

shows that this is not the case. At low velocities, the excitation probabilities for the atom ejected with $\theta \approx 50°$ are lower than those for the atom ejected with $\theta = 0°$. The reverse trend is observed at high velocities.

There are two mechanisms which are responsible for the observed differences in P. Consider first the low velocity regime. Figure 3 shows the variation of $v_\perp$ with height for the atoms ejected with two different polar angles ($\theta = 0°$ and $\theta \approx 50°$). The initial energy of the collision which started the ejection process was adjusted so that the particles in both cases would have the same final values of $v_\perp$. For this choice of $v_\perp$, the atom with $\theta \approx 50°$ has a smaller value of P. This deviation can be explained by examining the values of $v_\perp$ and $v_\parallel$ (the component of the velocity parallel to the surface) over the ejection trajectory. After the atom is set into motion, it moves at some nonzero initial polar angle, and thus $v_\parallel$ has some nonzero initial value. In the near-surface region, the atom's value of $v_\perp$ is smaller than that of the previous case ($\theta = 0°$), and so its initial excitation has more time to decay. The ejecting atom is then deflected by a neighboring atom. This deflection decreases the polar angle of ejection and causes $v_\perp$ to increase at the expense of $v_\parallel$. It is this same deflection which yields a final value of $v_\perp$ which is comparable to that of the previous case ($\theta = 0°$). This mechanism is similar to the binding energy effect in the sense that both processes cause $v_\perp$ to vary during the ejection event. The velocity of the atom is not constant during the ejection process and thus the final velocity is not a measure of the time the atom spends interacting with the solid.

The above mechanism can only exist at low collision velocities, where an atom ejecting with $\theta \approx 50°$ can get deflected by a neighboring atom at interatomic distances greater than r_{th}. A slight variation of this mechanism is present at high ejection (collision) velocities. At these velocities, this deflection can occur at interatomic distances which are less than r_{th}. Thus fast-moving atoms ejected with $\theta \approx 50°$ are simultaneously deflected and reexcited by neighboring atoms. An ejecting atom has to travel some distance before it encounters its neighbor, and gets reexcited at some distance (typically 0.5–1.0 Å) above the surface. We will refer to this event as a surface reexcitation. Since this reexcitation occurs a short distance above the surface, the deexcitation probability is less than if the excitation had occurred at the surface. This results in values of P for atoms ejected with off-normal angles which are greater in the high-velocity region than those for atoms ejected with $\theta = 0°$ (see Fig. 5).

In summary, calculations using the ideal case yield excitation probabilities which are similar to the experimental results at high $[(4\times10^5)$–(1×10^6) cm/s] ejection velocities. The calculations also show the existence of atomic deflections and/or collisions which can be used to qualitatively account for the increase of A/a with increasing polar angle of ejection. However, the ideal cases do not account for the existence of the constant excitation probabilities at low ($<4\times10^5$ cm/s) ejection velocities.

Simulations involving ion bombardment of the target and development of collision cascades were also performed. This calculation was performed in order to investigate the effect of disruption of the solid lattice on the excitation probabilities of the ejected atoms. All subsequent results presented in this section were obtained by calculating 4000 trajectory events (different ion bombardment events). The final excitation probabilities of the individual atoms ejected in three different directions are shown in Fig. 6. These are (a) normal to the surface ($\theta = 0°$–$20°$), (b) along the open azimuth ($\phi° = 0$, $30° < \theta < 50°$), and (c) along the close-packed direction ($\phi = 45°$, $30° < \theta < 50°$). There is a considerable amount of scatter in the results. This scatter is not noise or statistical uncertainty but is due to each ejected atom having a different history of excitations and subsequent relaxations. For a given value of $1/v_\perp$, one usually finds excitation probabilities ranging from $P_0 = 0.76$ (the upper limit of P) to the numerical integration limit of 10^{-6}. Less scatter in P can be seen at velocities above 4×10^5 cm/s. The results tend to cluster in a band around the values of P predicted by the calculations using the ideal case. For $\theta > 30°$ one finds a second band with values of P greater than the first one. This can be ascribed to the surface reexcitation of an ejecting atom when it is ejected at an angle and collides with a neighboring atom as described above.

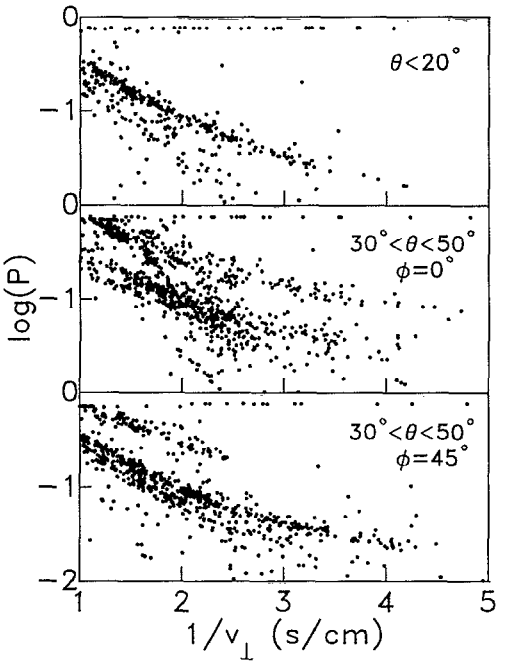

FIG. 6. Excitation probabilities obtained from computer simulations. Values of P for individual atoms are shown as a function of $1/v_\perp$. Data for three different directions of ejection are shown. These are (a) normal to the surface ($0° < \theta < 20°$), (b) along the open azimuth ($\phi = 0°$, $30° < \theta < 50°$), and (c) along the closed azimuth ($\phi = 45°$, $30° < \theta < 50°$).

Values of $(dN^*/dv)/(dN/dv)$ [obtained from Eq. (8)] for the above three sets of data are given in Fig. 7 as a function of $1/v_\perp$. Values of A/a at high velocities ($v_\perp > 4\times10^5$ cm/s) are between 0.5×10^6 and 0.8×10^6 cm/s. These values are smaller than the experimental values by about a factor of 2. This discrepancy is not surprising in

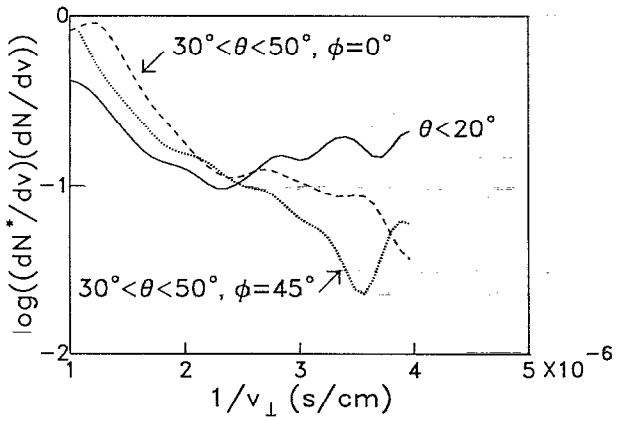

FIG. 7. Ratio of distributions, $(dN^*/dv)/(dN/dv)$, for the three sets of data given in Fig. 6.

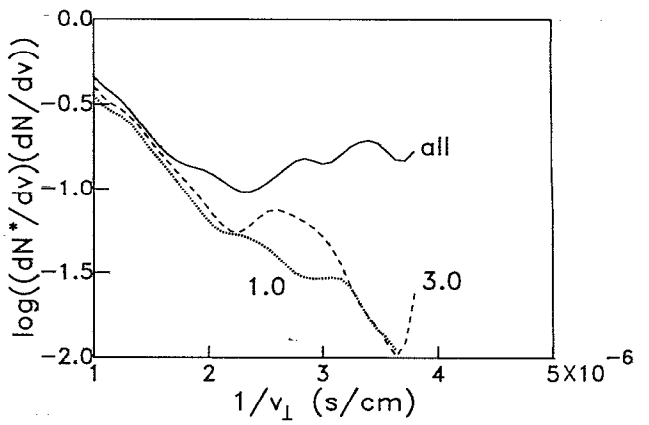

FIG. 9. Values of $(dN^*/dv)/(dN/dv)$ as a function of $1/v_\perp$. The solid line is obtained when all ejected atoms are used to calculate the average. The dashed line shows the average when all particles with $z_t > 3.0$ Å are excluded, while the dotted line is the average when all particles with $z_t > 1.0$ Å are excluded.

view of the fact that no exhaustive fit of the parameters in the model to the experimental data was attempted. At lower velocities, the behavior of $(dN^*/dv)/(dN/dv)$ switches from varying as $\exp(-A/av_\perp)$ to being constant. This behavior is in qualitative agreement with the experimental observations.

The mechanism responsible for the constant value of $(dN^*/dv)/(dN/dv)$ at low velocities can be deduced from results of the simulations. Examination of Fig. 6 shows that some atoms are ejected with final excitation probabilities equal to the initial value (P_0). At low velocities, these atoms make a significant contribution to the average excitation probability (the average being taken over all ejected atoms). How are these atoms with unusually high final values of P produced? Since molecular dynamics simulations allow us to study details of the atomic ejection processes, the excitation histories of these highly excited atoms can be examined. We find that these atoms are produced by collisions and reexcitations 1–20 Å above the surface. The height at which an atom is last excited, z_t, is plotted as a function of $1/v_\perp$ in Fig. 8. Most of the atoms are last excited at or near the surface. However, further analysis shows that ~11% of all ejected atoms undergo a collision 1–20 Å above the surface, and ~2.5% experience a collision 3–20 Å above the surface. (Both these numbers are supported by recent results from totally different simulations which were specifically designed to study collisions above the surface.[36]) If we recalculate $(dN^*/dv)/(dN/dv)$ while excluding atoms with $z_t > 3.0$ Å, then the contributions of these atoms reexcited above the surface to the total yield of excited atoms is decreased. The resulting $(dN^*/dv)/(dN/dv)$ is shown in Fig. 9. The region of constant $(dN^*/dv)/(dN/dv)$ starts to decrease, and the relationship between $\log[(dN^*/dv)/(dN/dv)]$ and $1/v_\perp$ approaches that of the ideal case over the whole range of velocities. If $(dN^*/dv)/(dN/dv)$ is recalculated with the exclusion of atoms with $z_t > 1.0$ Å, then the effects of above-surface reexcitations are further reduced. The result is a $\log[(dN^*/dv)/(dN/dv)] - 1/v_\perp$ relation which comes even closer to the predictions of the ideal case calculations for $\theta = 0°$.

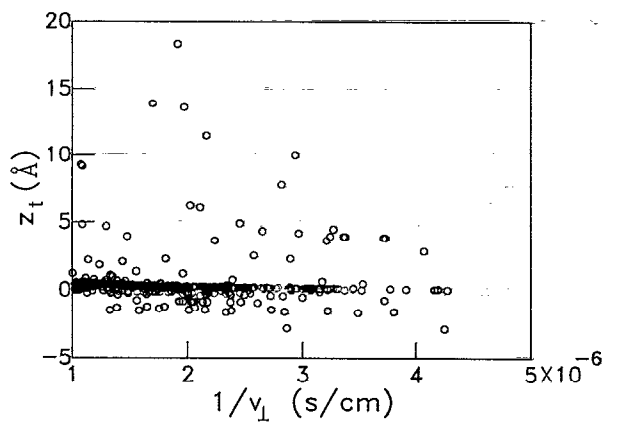

FIG. 8. Height at which an atom was last excited, z_t, as a function of $1/v_\perp$.

The simulations indicate that reexcitations 1–20 Å above the surface occur over the whole range of velocities studied. However, at high ejection velocities their contribution to the average value of P is masked by the large contribution from atoms excited at the surface. The importance of these above-surface reexcitations only becomes apparent at low velocities, where atoms excited at or near the surface have sufficient time to decay back to the ground state. At these low velocities ($v_\perp < 4\times10^5$ cm/s), about 40% of the excited atoms are produced via reexcitations at $z_t > 3.0$ Å.

In Sec. IV A it was mentioned that the constant value of $(dN^*/dv)/(dN/dv)$ at low velocities is dependent on both polar and azimuthal angles of emission. Unfortunately, examination of the angular dependence of the calculated excitation probability is hindered by poor statistics due to relatively few atoms ejected in excited states. Such detailed comparisons must be treated in simulations which are specifically designed to study collisions 1–20 Å above the surface.[36]

Using the current model, the simulations show that few excited atoms are produced by collisions below the surface (Fig. 8). We find that ~6% of all excited atoms originate from layers below the first one. This observation is in agreement with Shapiro and Fine's simulation[20] of inner shell excitations in Al. It is interesting to note that since they used a smaller value of r_{th} (0.521 Å) in simulating the more energetic inner shell excitations, they found that essentially all the excited atoms were the result of collisions between target atoms and the incident ion. We use a larger value of r_{th} (1.85 Å) and find that excited atoms are produced by collisions between two target atoms as well as collisions between a target atom and the incident ion.

In summary, the simulations involving realistic targets and ion bombardment events indicate that excitations 1–20 Å above the surface are responsible for the low velocity behavior of the excitation probability. This mechanism, in combination with the deflection and surface reexcitation mechanisms discovered in the ideal case calculations, accounts for the various angular and energy dependencies of $(dN^*/dv)/(dN/dv)$ which were observed in our experiments.

It is interesting to note that the nonradiative deexcitation formalism expresses P solely as a function of $v_\perp$. The fact that it, in conjunction with molecular dynamics simulations, can account for the angular dependence of P and $(dN^*/dv)/(dN/dv)$ presents a striking example of the success of simple models when they are combined with accurate and detailed descriptions of the system under study.

V. FUTURE WORK AND IMPLICATIONS

Future work is necessary to explore variations of the current excitation model and check the validity of some of the model's basic assumptions. One modification concerns the determination of an atom's initial excitation probability. In the current calculations, whenever an atom is collisionally excited, P is reset to an initial value P_0 regardless of its value before the collision. We plan to develop a more realistic scheme in which an atom's excitation is influenced by its previous excitations. A second modification involves using smaller values of r_{th}. This would decrease what appears to be an unusually large number of surface reexcitations which are shown in Fig. 6. Smaller values of r_{th} have been used in analogous simulations on the more closely packed Rh{111} face, and the preliminary results indeed show that decreasing r_{th} reduces the number of surface reexcitations.[36] These Rh{111} simulations also indicate that decreasing r_{th} or varying the lifetime of the excitation does not change the general behavior of $(dN^*/dv)/(dN/dv)$ with velocity.

The study of systems with multiple excitation levels having various values of r_{th} represents another extension of the present work. Preliminary studies on Rh{111} indicate that the presence of these levels leads to additional peaks in the excited-atom velocity distributions. The velocities at which these maxima occur are roughly inversely proportional to the value of r_{th}. This finding is not surprising since smaller values of r_{th} correspond to levels with higher excitation energies.

It has been suggested that excited atoms can undergo Auger decay to become secondary ions.[37,38] In this case, some of the findings in this study may apply to the ejection of ions from keV particle-bombarded clean metals. For instance, collisional effects could lead to a nonexponential $(1/v_\perp)$ dependence of the ionization probability at low velocities, thus explaining experimental data[39] which indicate that the dependence should be v^n where $n=0$–2.

ACKNOWLEDGMENTS

The financial support of the National Science Foundation, the Office of Naval Research, and the IBM Program for the Support of the Materials and Processing Sciences are gratefully acknowledged. B.J.G. also acknowledges the Camille and Henry Dreyfus Foundation for a Teacher–Scholar Award. Z.P. thanks the Polish Ministry of Sciences Project No. CPBR-01-09 for additional support. The Pennsylvania State University supplied an extremely generous grant of computer time for these calculations.

[1] B. J. Garrison, N. Winograd, D. M. Deaven, C. T. Reimann, D. Y. Lo, T. A. Tombrello, D. E. Harrison, Jr., and M. H. Shapiro, Phys. Rev. B **37**, 7197 (1988).
[2] R. Maboudian, Z. Postawa, M. El-Maazawi, B. J. Garrison, and N. Winograd, Phys. Rev. B **42**, 7311 (1990).
[3] C. Snoek, W. F. van der Weg, and P. K. Rol, Physica (Utrecht) **30**, 341 (1964).
[4] W. F. van der Weg and D. J. Bierman, Physica (Utrecht) **44**, 206 (1969).
[5] C. W. White and N. H. Tolk, Phys. Rev. Lett. **26**, 486 (1971).
[6] S. Dzioba, O. Auciello, and R. Kelly, Radiat. Eff. **45**, 235 (1980).
[7] S. Dzioba and R. Kelly, Surf. Sci. **100**, 119 (1980).
[8] R. B. Wright and D. M. Gruen, J. Chem. Phys. **72**, 147 (1980).
[9] I. S. T. Tsong and N. A. Yusuf, Nucl. Instrum. Methods **170**, 357 (1980).
[10] M. J. Pellin, R. B. Wright, and D. M. Gruen, J. Chem. Phys. **74**, 6448 (1981).
[11] C. M. Loxton and R. J. MacDonald, Surf. Sci. **110**, 339 (1981).
[12] M. L. Yu, D. Grischkowsky, and A. C. Balant, Phys. Rev. Lett. **48**, 427 (1982).
[13] W. Husinsky, G. Betz, and I. Girgis, Phys. Rev. Lett. **50**, 1689 (1983).
[14] G. Betz, Nucl. Instrum. Methods Phys. Res. Sect. B **27**, 104 (1987).
[15] B. I. Craig, J. P. Baxter, J. Singh, G. A. Schick, P. H. Kobrin, B. J. Garrison, and N. Winograd, Phys. Rev. Lett. **57**, 1351 (1986).
[16] M. El-Maazawi, R. Maboudian, Z. Postawa, and N. Winograd, Phys. Rev. B **43**, 12 078 (1991).
[17] N. Winograd, M. El-Maazawi, R. Maboudian, Z. Postawa, D. N. Bernardo, and B. J. Garrison, J. Chem. Phys. **96**, 6314 (1992).
[18] H. D. Hagstrum, Phys. Rev. **96**, 336 (1954).
[19] C. W. White, D. L. Simms, N. H. Tolk, and D. V. McCaughan, Surf. Sci. **49**, 657 (1975).
[20] M. H. Shapiro and J. Fine, Nucl. Instrum. Methods Phys. Res. Sect. B **44**, 43 (1989).
[21] J. J. Vrakking and A. Kroes, Surf. Sci. **84**, 153 (1979).
[22] D. Grischkowsky, M. L. Yu, and A. C. Balant, Surf. Sci. **127**, 351 (1983).
[23] M. L. Yu and N. D. Lang, Phys. Rev. Lett. **50**, 127 (1983).
[24] J. H. Lin and B. J. Garrison, J. Vac. Sci. Technol. A **1**, 1205 (1983).
[25] B. J. Garrison, Surf. Sci. **167**, L225 (1986).
[26] N. D. Lang, Phys. Rev. B **27**, 2019 (1983).
[27] M. L. Yu and N. D. Lang, Nucl. Instrum. Methods Phys. Res. Sect. B **14**, 403 (1986).
[28] Equation (6) is based on the assumption that the populations of the higher-lying excited states are sufficiently small as to render cancade transitions negligible. Our probing of the next higher-lying excited state

($^4F_{5/2}$, with excitation energy of 0.3 eV above the ground state) reveals its population to be at least 2 orders of magnitude smaller than that of the first excited state. Since the population density of a given level decays exponentially with the excitation energy [F. M. Kimock, J. P. Baxter, D. L. Pappas, P. H. Kobrin, and N. Winograd, Anal. Chem. **56**, 2782 (1984)], we can conclude that cascade transitions are insignificant in our system.

[29] P. H. Kobrin, G. A. Schick, J. P. Baxter, and N. Winograd, Rev. Sci. Instrum. **57**, 1354 (1986).

[30] M. Dupuis, J. D. Watts, H. O. Villar, and G. J. B. Hurst, HONDO7, Quantum Chemistry Program Exchange Program 544 (1987).

[31] P. J. Hay and W. R. Wadt, J. Chem. Phys. **82**, 270 (1985).

[32] U. Fano and W. Lichten, Phys. Rev. Lett. **14**, 627 (1965).

[33] C. Kittel, *Introduction to Solid State Physics*, 6th ed. (Wiley, New York, 1986), p. 24.

[34] F. Illas, J. Rubio, J. Cañellas, and J. M. Ricart, J. Chem. Phys. **93**, 2603 (1990).

[35] We assume that the interatomic distances in multimers are similar in value to those in the bulk and dimers.

[36] D. N. Bernardo and B. J. Garrison (unpublished results).

[37] P. Joyes, J. Phys. (Paris) **29**, 774 (1968).

[38] V. I. Veksler, Sov. Phys. Solid State **24**, 997 (1982).

[39] See, for example, R. A. Gibbs, S. P. Holland, K. E. Foley, B. J. Garrison, and N. Winograd, J. Chem. Phys. **76**, 684 (1982).